



Research papers

Projecting potential evapotranspiration change and quantifying its uncertainty under future climate scenarios: A case study in southeastern Australia



Lijie Shi^{a,b}, Puyu Feng^{a,b}, Bin Wang^{b,*}, De Li Liu^{b,c,*}, James Cleverly^a, Quanxiao Fang^d, Qiang Yu^{d,a,e,*}

^a School of Life Sciences, Faculty of Science, University of Technology Sydney, PO Box 123, Broadway, Sydney, NSW 2007, Australia

^b NSW Department of Primary Industries, Wagga Wagga Agricultural Institute, Wagga Wagga, NSW 2650, Australia

^c Climate Change Research Centre and ARC Centre of Excellence for Climate System Science, University of New South Wales, Sydney, NSW 2052, Australia

^d State Key Laboratory of Soil Erosion and Dryland Farming on the Loess Plateau, Northwest A&F University, Yangling, Shaanxi 712100, China

^e College of Resources and Environment, University of Chinese Academy of Science, Beijing 100049, China

ARTICLE INFO

This manuscript was handled by G. Syme, Editor-in-Chief, with the assistance of Ji Chen, Associate Editor

Keywords:

Potential evapotranspiration
Empirical ETP models
Random forest
Uncertainty
Climate change
Southeastern Australia

ABSTRACT

Projecting the likely change of potential evapotranspiration (ETp) under future climate scenarios is crucial for quantifying the impacts of climate change on the hydrologic cycle and aridity conditions. However, there are different sources of uncertainty in projecting future ETp that may arise from global climate models (GCMs), emission scenarios, and multiple ETP models used. In this study, we developed three random forest-based (RF-based) ETP models with solar radiation and air temperature at eight climatic stations in southeastern Australia. With Penman model as the benchmark, their performance was firstly compared with four empirical models (Jensen-Haise, Makkink, Abtew, and Hargreaves), which requires the same meteorological inputs. In general, the RF-based ETP models showed better performance in ETP estimates across all stations, with coefficients of determination (R^2) ranging from 0.68 to 0.92, root mean square errors (RMSE) ranging from 0.58 mm day⁻¹ to 1.46 mm day⁻¹, and relative mean bias errors (rMBE) ranging from -16.10% to 9.73%. The RF-based and empirical models were then used to project future ETP for the eight stations based on statistically downscaled daily climatic data from 34 GCMs under two different representative concentration pathways (RCP4.5 and RCP8.5). All models indicated that ETP was likely to increase at the eight stations. The ensemble increases of mean ETP across eight stations ranged from 33 mm year⁻¹ (2.1%, 2040s) to 129 mm year⁻¹ (9.2%, 2090s) and from 43 mm year⁻¹ (2.8%, 2040s) to 248 mm year⁻¹ (17.6%, 2090s) under RCP4.5 and under RCP8.5, respectively. In addition, we also quantified uncertainties in ETP projections originating from ETP models, GCMs, RCPs, and their combined effects using the analysis of variance (ANOVA) method. Results showed that RCP-related uncertainty contributed the most to projected ETP uncertainty (around 40% for most stations) while GCM-related and ETP model-related uncertainties accounted for roughly equal amounts of projected ETP uncertainty (10%–30%). This study demonstrated the better performance of RF-based ETP models. It is advisable to use multiple ETP models driven by various GCMs under different RCPs to produce reliable projections of future ETP.

1. Introduction

The hydrological cycle has intensified in the last century and the rate of intensification for the coming century is accelerating due to climate change (Durack et al., 2012; Pan et al., 2015). This may lead to a global shift in aridity or make dry regions become drier while wet

regions become wetter (Chen et al., 2017). Thus, it is important to investigate the influence of climate change on the water cycle. As one of the most important components of hydrological and climatological processes, evapotranspiration (ET) accounts for around 70% of precipitation falling on land and consumes more than 50% of the solar energy absorbed by the earth (Guo et al., 2017; Pan et al., 2015;

* Corresponding authors at: State Key Laboratory of Soil Erosion and Dryland Farming on the Loess Plateau, Northwest A&F University, Yangling, Shaanxi 712100, China; NSW Department of Primary Industries, Wagga Wagga Agricultural Institute, Wagga Wagga, NSW 2650, Australia.

E-mail addresses: bin.a.wang@dpi.nsw.gov.au (B. Wang), de.li.liu@dpi.nsw.gov.au (D. Li Liu), yuq@nwfafu.edu.cn (Q. Yu).

<https://doi.org/10.1016/j.jhydrol.2020.124756>

Received 3 September 2019; Received in revised form 6 January 2020; Accepted 21 February 2020

Available online 24 February 2020

0022-1694/ © 2020 Elsevier B.V. All rights reserved.

Vicente-Serrano et al., 2014). Thus, ET is a very useful indicator to analyse the changing behaviour of the hydrologic regime (Wang et al., 2017b).

However, ET is not easy to measure. For instance, although lysimeters are frequently used to directly measure ET, they are sparsely distributed around the world because they are expensive and laborious to manage (Azhar and Perera, 2011). Therefore, ET is generally estimated by various empirical models that estimate either potential evapotranspiration (ETp) or reference evapotranspiration (ETO) (Almorox et al., 2015). ETp represents the maximum possible evapotranspiration rate from a well-watered, vegetative surface (Donohue et al., 2010; McMahon et al., 2016), and is regarded as the optimum measurement of evaporative demand from actual land surfaces under specified meteorological conditions (Zheng et al., 2017). In fact, ETp (rather than actual ET) has been widely used as an important input to various hydrological models (Thompson et al., 2013) and aridity indexes (Sheffield et al., 2012). In general, ET models can be classified into four categories according to their input requirements, i.e. temperature-based models (Hargreaves et al., 1985), radiation-based models (Jensen and Haise, 1963; Makkink, 1957), mass transfer-based models (Mahringer, 1970), and combination models (Penman, 1948). Among them, the Penman model and the FAO56 Penman-Monteith (PM-FAO56) model are two variants of the Penman-Monteith-type models. They are both physically-based models (Milly and Dunne, 2016; Yang et al., 2019) that can accurately estimate ET across various climate conditions (Donohue et al., 2010; Milly and Dunne, 2016). Therefore, they are widely used as benchmarks to assess the performance of other ETp/ETO models. In contrast to the Penman model, PM-FAO56 considers the surface conductance of a reference crop, and provides estimates of ETO while the Penman model provides estimates of ETp. Both of these models require the complete set of climatic data, which may limit their use in some regions. In the particular case of future ET projection, downscaled climatic data, such as wind speed and relative humidity, may not be reliable (Randall et al., 2007), thus limiting the use of Penman-Monteith-type models.

Compared with the Penman model, simplified empirical ETp models require fewer climate inputs to offer acceptable estimates (Almorox et al., 2015). These empirical ETp models (e.g., temperature-based models) may be preferable for future ETp projection because GCM-simulated temperature is considered to have higher confidence than other climatic variables (CSIRO and BOM, 2015; Randall et al., 2007). For instance, Kay and Davies (2008) used both the Penman-Monteith model and a temperature-based model to estimate ETp of Britain with climate data from five GCMs and eight regional climate models. They demonstrated that ETp estimated by the temperature-based model with temperature from a climate model matched MORECS ETp (a gridded dataset of estimated ETp based on observed climatic data with the Penman-Monteith model) better than ETp estimated by the Penman-Monteith model with climate model data. Similarly, Ravazzani et al. (2014) adopted a temperature-based model and an energy balance-based ETp model which requires a complete set of climate data to quantify the influence of climate change on water resources in Northern Italy. They found that a simple temperature-based ETp model is sufficiently accurate for analysing the climate change effects on hydrological regimes.

In addition to empirical ETp models, newly emerging machine learning techniques have recently been used to estimate ETp (Feng et al., 2018; Kisi, 2015; Kişi, 2013; Kisi and Alizamir, 2018; Mehdizadeh, 2018; Tabari et al., 2012; Wang et al., 2017a). The major advantage of machine learning techniques is that they are capable of tackling non-linear relationships between the dependent and independent variables without requiring knowledge of the internal variables (Fan et al., 2018; Mehdizadeh, 2018). Performance comparisons between machine learning techniques and conventional empirical models for estimating ET have been widely reported. For instance, Tabari et al. (2012) evaluated the performance of support vector

machines (SVM), adaptive neuro-fuzzy inference systems (ANFIS), multiple linear regression, multiple non-linear regression, four temperature-based ETO models, and eight radiation-based ETO models for estimating ETO compared with the PM-FAO56 model in a semi-arid highland environment in Iran. They found that SVM and ANFIS performed better than the regression-based models and the corresponding conventional ETO models (i.e., models requiring the same climatic inputs). In the Poyang Lake Watershed, Lu et al. (2018) adopted three tree-based machine learning methods including M5Tree, random forest (RF), and gradient boosting decision tree (GBDT) and four empirical models to estimate pan evaporation from 2001 to 2015. They found machine learning models, especially GBDT and RF, showed great potential for estimating daily pan evaporation regardless of the input combination. In Spain, Shiri et al. (2012) assessed the performance of Gene Expression Programming (GEP), ANFIS, Hargreaves, and Priestley-Taylor for calculating daily ETO compared with the PM-FAO56 model and found that both GEP and ANFIS performed better than the two conventional models. In summary, machine learning models generally outperformed conventional empirical models (i.e., for models requiring the same climatic inputs) in accurately estimating ET. However, their use in projecting future ETp is still rare.

Another widely discussed problem in the estimation of future ETp is related to the uncertainty generated by various ETp models, GCMs, and emission scenarios (Bae et al., 2011; Wilby and Harris, 2006; Xu et al., 2014). For instance, Wang et al. (2015) found that the directly downscaled ETp values from HadCM3 and ETp estimated by PM-FAO56 and Hargreaves models would all increase under future climate scenarios in the Hanjiang River Basin. However, the magnitudes of the ETp increases varied greatly among these ETp models, up to 70 mm year⁻¹. Other researchers (Arnell and Gosling, 2013; Kay and Davies, 2008) also reported that the projected ETp under future climate scenarios could be significantly different due to the differences in GCMs and ETp models, indicating the large uncertainty in future ETp projections. Thus, it is necessary to quantify the uncertainty originating from various sources in order to evaluate the reliability of ETp projections. Thompson et al. (2014) concluded that GCM-related uncertainty was about 3.5 times larger than ETp model-related uncertainty for the projection of river flow in the Mekong River Basin. For the projection of future global ETp with various ETp models and GCMs, Kingston et al. (2009) claimed that ETp model-related uncertainty was equal to or, in some circumstance, greater than GCM-related uncertainty. However, to our knowledge, few studies have systematically quantified the uncertainties originating from conventional ETp models as well as machine learning-based models, GCMs, emission scenarios, and their combined effects.

Australia is a water-scarce and drought-vulnerable country (Howden et al., 2014; Verdon-Kidd and Kiem, 2009). The warming climate may exacerbate the water-scarce situation in this region. Therefore, studying the likely change of ETp in Australia is necessary for the development of proposals and policies for adapting water management to climate change. In this study, we first proposed a machine learning method to estimate ETp in southeastern Australia and used multiple ETp models driven by statistically downscaled climate data from a large number of GCMs to quantify the impacts of climate change on ETp. The objectives of this study were to 1) assess the performance of machine learning-based ETp models for estimating daily ETp; 2) explore the likely change of future ETp in the study area based on various ETp models; and 3) quantify the contributions of different sources of uncertainty, including GCMs, ETp models, emission scenarios, and their combined effects, to the uncertainty in future ETp projections. This research will provide a good reference for researchers to better understand the performance of machine learning-based ETp models in projecting future ETp. Additionally, knowledge of the uncertainty in future ETp projections would also help researchers to understand the potential bias in projecting the hydrological cycle and water availability under future climate scenarios.

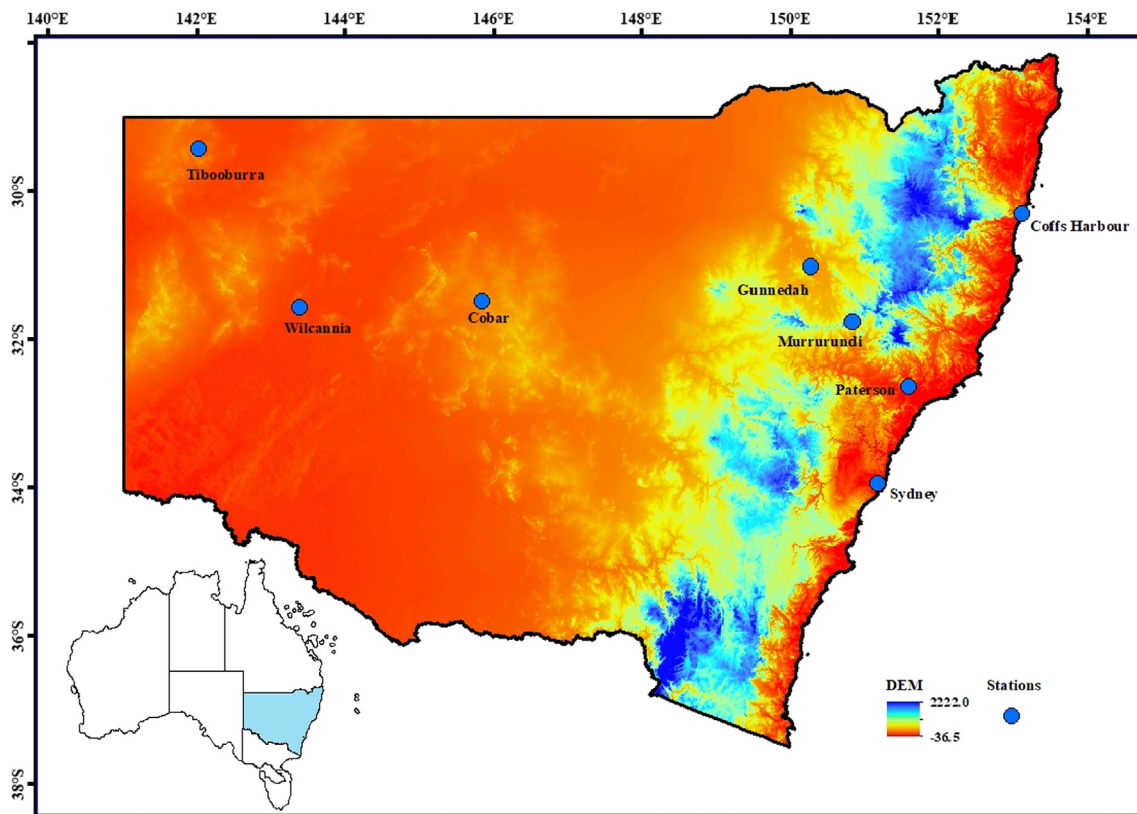


Fig. 1. The location of eight stations in New South Wales, Australia, and their elevations (m) determined by digital elevation model (DEM).

Table 1

Geographical and long-term average meteorological information for eight stations in New South Wales, Australia. The values in parentheses are the standard deviations for each variable.

| | Lon (°E) | Lat (°S) | DEM (m) | T ^a (°C) | Rs ^b (MJ m ⁻² d ⁻¹) | RH ^c (%) | Wind ^d (m/s) | VPD ^e (kpa) | Rainfall (mm) | ETp (mm) | AI ^f | Period |
|---------------|-------------|-------------|------------|------------------------|--|------------------------|----------------------------|---------------------------|------------------|-------------|-----------------|-----------|
| Tibooburra | 142 | -29.4 | 183 | 20.8 (0.7) | 20.8 (0.7) | 48.1 (4.4) | 2.4 (1.0) | 1.8 (0.2) | 248 (143) | 2133 (267) | 0.12 (0.08) | 1953–2014 |
| Wilcannia | 143.4 | -31.6 | 75 | 19.5 (0.5) | 19.7 (0.6) | 55.3 (3.7) | 2.7 (0.6) | 1.6 (0.2) | 272 (126) | 2072 (173) | 0.14 (0.07) | 1957–2014 |
| Cobar | 145.8 | -31.5 | 260 | 19.0 (0.7) | 19.4 (0.7) | 54.4 (4.6) | 2.1 (0.5) | 1.5 (0.2) | 397 (156) | 1865 (171) | 0.22 (0.10) | 1963–2014 |
| Gunnedah | 150.3 | -31 | 307 | 18.3 (0.6) | 18.6 (0.7) | 63.3 (3.3) | 1.8 (0.3) | 1.1 (0.1) | 632 (161) | 1639 (102) | 0.39 (0.11) | 1951–2014 |
| Murrurundi | 150.8 | -31.8 | 466 | 15.5 (0.5) | 17.5 (0.7) | 71.2 (2.7) | 1.6 (0.4) | 0.9 (0.1) | 857 (197) | 1429 (122) | 0.61 (0.17) | 1965–2014 |
| Paterson | 151.6 | -32.6 | 30 | 18.0 (0.5) | 16.9 (0.5) | 71.5 (1.9) | 2.3 (0.5) | 0.9 (0.1) | 930 (196) | 1533 (107) | 0.61 (0.15) | 1968–2014 |
| Sydney | 151.2 | -34 | 6 | 17.9 (0.7) | 16.4 (0.5) | 68.6 (3.0) | 3.1 (0.8) | 0.8 (0.1) | 1123 (309) | 1551 (154) | 0.74 (0.25) | 1950–2014 |
| Coffs Harbour | 153.1 | -30.3 | 5 | 18.7 (0.5) | 17.4 (0.6) | 72.6 (1.6) | 2.7 (0.4) | 0.7 (0.1) | 1720 (467) | 1539 (85) | 1.13 (0.34) | 1952–2014 |

^a Air temperature.

^b Solar radiation.

^c Relative humidity.

^d Wind speed.

^e Vapor pressure deficit.

^f Aridity index calculated as rainfall/ETp.

2. Materials and methods

2.1. Study area

New South Wales (NSW) is located in southeast Australia (Fig. 1). It accounts for 10.4% of the Australian land area ($8.1 \times 10^5 \text{ km}^2$) and has a population of more than eight million, making NSW the most populous state in Australia. The production of agricultural crops in NSW is important to the agricultural industry in Australia. For instance, wheat grown in NSW accounts for 28% of the total wheat-planted area in Australia (Feng et al., 2019b). However, topography and climatic characteristics in NSW vary greatly from east to west, making it vulnerable to climate change. In general, NSW can be divided into four distinct geographical sections based on their natural features, namely

the east coast, the mountains, the central plains, and the western plains. Climatically, the east coast and the mountains are characterized by humid or sub-humid climates while the central and western plains experience semi-arid or arid climates. Average annual rainfall gradually increases from 50 mm year^{-1} in the westernmost region to $1500 \text{ mm year}^{-1}$ on the east coast. Similarly, average annual temperature gradually increases from around 10 °C in the southeast to greater than 20 °C in the northwest.

Climate in NSW is expected to change under the influence of future global warming. For instance, temperature in NSW is projected to rise by 2.1 °C by 2070 while annual rainfall is likely to decrease (CSIRO and BOM, 2015; Vaze et al., 2008). Furthermore, extreme weather events such as heatwaves and droughts may occur more frequently (Feng et al., 2019a), which might exacerbate water scarcity in NSW and result in

new water management challenges. Thus, it is necessary to project ETp changes under future climate scenarios to predict the effects of climate change on water resource management and drought prediction.

Eight stations in NSW (Fig. 1) were selected for examination in this study because they have complete sets of climate data that are required for the Penman model to estimate daily ETp. Geographic information, ETp-related climate variables, annual rainfall, and aridity index of these stations are shown in Table 1.

2.2. Climate data and downscaling method applied

Historical daily climate data during the research period, including maximum temperature (T_{\max}), minimum temperature (T_{\min}), maximum and minimum relative humidity (RH_{\max} and RH_{\min} , respectively), rainfall, and solar radiation (R_s), were obtained from the Scientific Information for Land Owners (SILO) patched point dataset (<https://www.longpaddock.qld.gov.au/silo/datadrill/index.php>). In addition, wind speed data were obtained from the Bureau of Meteorology (BOM, <http://www.bom.gov.au/>). The percentage of missing daily wind speed data was less than 5% for each station. To estimate the missing wind speed values, we first used years with consecutive daily wind speed to calculate the long-term average wind speed for each day of the year. Then we used the average wind speed for the i -th (i ranges from 1 to 365) day of the year as the proxy wind speed for that day of the year with a missing value. To project ETp under future climate scenarios, we downscaled 34 GCMs (Table 2) from the Coupled Model Inter-comparison Project Phase 5 (CMIP5) dataset to extract daily T_{\max} , T_{\min} , rainfall, and R_s from 1900 to 2100 based on the statistical downscaling method developed by Liu and Zuo (2012).

Statistical downscaling is an effective method to downscale the raw

Table 2

Identifying information for 34 global climate models (GCMs). GCMs were used for statistically downscaling outputs for eight stations across New South Wales, Australia, under the RCP4.5 and RCP8.5 scenarios.

| Model ID | Name of GCM | Abbr. of GCM | Institute ID | Country |
|----------|----------------|--------------|---------------|-----------|
| 1 | ACCESS1-0 | AC1 | CSIRO and BoM | Australia |
| 2 | ACCESS1-3 | AC2 | CSIRO and BoM | Australia |
| 3 | BCC-CSM1-1 | BC1 | BCC | China |
| 4 | BCC-CSM1-1-m | BC2 | BCC | China |
| 5 | BNU-ESM | BNU | GCESS | China |
| 6 | CanESM2 | CaE | CCMA | Canada |
| 7 | CCSM4 | CCS | NCAR | USA |
| 8 | CESM1-BGC | CE1 | NSF-DOE-NCAR | USA |
| 9 | CESM1-CAM5 | CE2 | NSF-DOE-NCAR | USA |
| 10 | CESM1-WACCM | CE5 | NSF-DOE-NCAR | USA |
| 11 | CMCC-CM | CM2 | CMCC | Europe |
| 12 | CMCC-CMS | CM3 | CMCC | Europe |
| 13 | CNRM-CM5 | CN1 | CNRM-GAME | France |
| 14 | CSIRO-Mk3-6-0 | CSI | CSIRO-QCCCE | Australia |
| 15 | EC-EARTH | ECE | EC-EARTH | Europe |
| 16 | FIO-ESM | FIO | FIO | China |
| 17 | GISS-E2-H | GE1 | NASA GISS | USA |
| 18 | GISS-E2-H-CC | GE2 | NASA GISS | USA |
| 19 | GISS-E2-R | GE3 | NASA GISS | USA |
| 20 | GFDL-CM3 | GF2 | NOAA GFDL | USA |
| 21 | GFDL-ESM2G | GF3 | NOAA GFDL | USA |
| 22 | GFDL-ESM2M | GF4 | NOAA GFDL | USA |
| 23 | HadGEM2-AO | Ha5 | NIMR/KMA | Korea |
| 24 | INM-CM4 | INC | INM | Russia |
| 25 | IPSL-CM5A-LR | IP1 | IPSL | France |
| 26 | IPSL-CM5A-MR | IP2 | IPSL | France |
| 27 | IPSL-CM5B-LR | IP3 | IPSL | France |
| 28 | MIROC5 | MI2 | MIROC | Japan |
| 29 | MIROC-ESM | MI3 | MIROC | Japan |
| 30 | MIROC-ESM-CHEM | MI4 | MIROC | Japan |
| 31 | MPI-ESM-LR | MP1 | MPI-M | Germany |
| 32 | MRI-CGCM3 | MR3 | MRI | Japan |
| 33 | NorESM1-M | NE1 | NCC | Norway |
| 34 | NorESM1-ME | NE2 | NCC | Norway |

monthly climatic data from GCMs at coarse spatial resolutions to a finer spatial and temporal scale. Firstly, the monthly climatic data from GCMs were downscaled to specific sites using the inverse distance weighted interpolation method. Then bias correction was applied to the monthly values of climatic factors for each site. Thirdly, we used a stochastic weather generator to produce daily climatic factors for each site. The detailed information about this method has been described by Liu and Zuo (2012). This study used the downscaled data to project future ETp with the chosen empirical and machine learning-based ETp models under RCP4.5 and RCP8.5 climate scenarios.

For data downscaled from 34 GCMs, we defined the period from 1990 to 2014 as the baseline period. The near future projected period was defined as 2026 to 2050 (2040s); the medium projected period was from 2051 to 2075 (2065s); and the far future period was 2076–2100 (2090s).

2.3. The Penman model

As mentioned in the Introduction, the Penman model is widely used as a benchmark to assess the performance of other ETp models. In this study, we also assessed the performance of other models against the Penman model. The mathematical expression of the Penman model is shown in Eq. (1):

$$ET_{p, Penman} = \frac{0.408\Delta}{\Delta + \gamma} (R_n - G) + \frac{\gamma}{\Delta + \gamma} \frac{6.43(1 + 0.536u_2)(e_s - e_a)}{\lambda} \quad (1)$$

where $ET_{p, Penman}$ (mm day⁻¹) is Penman-calculated ETp. Δ (kPa °C⁻¹) is the slope of the saturation vapor pressure curve, determined by air temperature (T), as shown in Eq. (2); γ (kPa °C⁻¹) is the psychrometric constant; R_n (MJ m⁻² day⁻¹) is net radiation determined according to Allen et al. (1998) and shown in Eq. (3). G (MJ m⁻² day⁻¹) is soil heat flux density, assumed to equal zero for periods of a day or longer (Allen et al., 1998; Irmak et al., 2012); u_2 (m s⁻¹) is wind speed at 2 m height; e_s (kPa) is saturation vapor pressure, determined by air temperature; e_a (kPa) is actual vapor pressure, determined by air temperature and relative humidity; $(e_s - e_a)$ (kPa) is saturation vapor pressure deficit; and λ is the latent heat of vaporisation of water, which is calculated as a function of T, value of 2.45 MJ kg⁻¹ for T around 20 °C.

$$\Delta = \frac{4098 \times \left[0.6108 \exp\left(\frac{17.27T}{T + 237.3}\right) \right]}{(T + 237.3)^2} \quad (2)$$

where T (°C) is mean daily air temperature at 2 m height.

$$R_n = R_{ns} - R_{nl} \quad (3)$$

where R_{ns} (MJ m⁻² day⁻¹) is the shortwave radiation, as shown in Eq. (4); R_{nl} (MJ m⁻² day⁻¹) is the longwave radiation, as shown in Eq. (5),

$$R_{ns} = (1 - \alpha)R_s \quad (4)$$

where α is albedo, which is influenced by the surface characteristics and the angle or slope of the ground surface. For a green vegetation surface, α varies from 0.20 to 0.25. In this study, $\alpha = 0.23$, as recommended by Allen et al. (1998) for a hypothetical green surface. R_s (MJ m⁻² day⁻¹) is the solar radiation.

$$R_{nl} = 4.903 \times 10^{-9} \times \left(\frac{(T_{\max} + 273.06)^4 + (T_{\min} + 273.06)^4}{2} \right) \times (0.34 - 0.14\sqrt{e_a}) \times \left(1.35 \times \frac{R_s}{R_{so}} - 0.35 \right) \quad (5)$$

where T_{\min} (°C) and T_{\max} (°C) are the minimum and maximum temperature, respectively; R_{so} (MJ m⁻² day⁻¹) is the clear-sky radiation, estimated by extraterrestrial radiation (R_a).

2.4. Four empirical ETp models

Priestley and Taylor (1972) and Samani (2000) reported that air

temperature and solar radiation could explain at least 80% of variations in ETp (Almorox et al., 2015). Most GCMs have reliable prediction of air temperature. Therefore, we also adopted commonly used temperature-based and radiation-based models to compare their performance with random forest-based ETp models, and to project future ETp. The temperature-based model used in this study was the well-known Hargreaves (HS) model, and the three radiation-based models were Jensen-Haise (JH), Makkink (Mak), and Abtew (Ab). Their mathematical expressions were as follows:

$$ET_{p,HS} = 0.0023 \times 0.408R_a(T_{\max} - T_{\min})^{0.5}(T + 17.8) \quad (6)$$

$$ET_{p,JH} = 0.0102(T + 3)R_s \quad (7)$$

$$ET_{p,Mak} = 0.7 \frac{\Delta}{\Delta + \gamma} \frac{R_s}{\lambda} \quad (8)$$

$$ET_{p,Ab} = 0.01786 \frac{R_s T_{\max}}{\lambda} \quad (9)$$

parameters in these models have the same definitions as used above in the Penman model.

2.5. Random forest-based ETp models

Random forest (RF) is one of the tree-based machine learning methods developed by Breiman (2001). Compared with most well-established machine learning methods (e.g., artificial neural networks and SVM), RF only needs two parameters: the number of decision trees (n_{tree}) and the number of variables (m_{try}). Moreover, RF has a strong predictive power to deal with non-linear and hierarchical relationships between the predictors and the response. In fact, RF has been widely used for classification and regression tasks (Fan et al., 2018; Heung et al., 2014; Wang et al., 2018b). Thus, we adopted RF as a representative machine learning technique to estimate ETp in this study. Briefly, around 2/3 of the original data were randomly chosen as the “bootstrapped” dataset to generate numerous decision trees (n_{tree}) with a random subset of the total variables (m_{try}) each step. Thus, a variety of decision trees were generated that formed the “Forest”. The remaining original data (around 1/3), which were not chosen to build the “bootstrapped” dataset (known as the “Out-of-Bag Dataset”) were used for validation. Based on the “Forest”, the projector used predicted data and ran those data through all of the decision trees. The final prediction was the average of the results of all trees. More information about RF can be found in Breiman (2001), and a schematic diagram of RF is shown in Fig. S1.

This study adopted the “randomForest” package in R (Liaw and Wiener, 2002) (<https://cran.r-project.org/web/packages/randomForest/index.html>) to develop RF-based ETp models with observed historical climatic data. The daily climatic data from 1950 (or the starting year of the station shown in Table 1) to 2000 were used to train RF-based ETp models while the data from 2001 to 2014 were used to test these RF-based ETp models. Three RF-based ETp models (Table 3) were developed, namely RF1 based on T_{\max} , T_{\min} , and R_s to compare with JH and Mak; RF2 based on T_{\max} , T_{\min} , and extra-terrestrial solar radiation (R_a) to compare with HS; and RF3 based on T_{\max} and R_s to compare with Ab. We set n_{tree} as 500 to ensure that every input row would be predicted a few times. The default value of m_{try} is generally around 1/3 of the number of input variables (p) (Guio Blanco et al., 2018). Because of the small number of input variables in the current study, we used m_{try} values which were somewhat larger than 0.33p. The number of predictors in our study was 3 for RF1 and RF2, and 2 for RF3. Thus, we set m_{try} as 2 for RF1 and RF2, and 1 for RF3.

2.6. Model evaluation

Performance (with regards to estimates of ETp rates) of RF-based (RF1, RF2, and RF3) and empirical (JH, Mak, HS, and Ab) ETp models

Table 3

The input requirements of seven ETp models used in this study.

| Models | Inputs |
|-------------------|---------------------------------|
| RF1 | $T_{\max}^a, T_{\min}^b, R_s^c$ |
| Jensen-Haise (JH) | T_{\max}, T_{\min}, R_s |
| Makkink (Mak) | T_{\max}, T_{\min}, R_s |
| RF2 | $T_{\max}, T_{\min}, R_a^c$ |
| Hargreaves (HS) | $T_{\max}, T_{\min}, R_a^d$ |
| RF3 | T_{\max}, R_s |
| Abtew (Ab) | T_{\max}, R_s |

^a Maximum air temperature.

^b Minimum air temperature.

^c Solar radiation.

^d Extraterrestrial solar radiation.

was evaluated against the Penman model with the commonly used statistical parameters: coefficient of determination (R^2), root mean square error (RMSE, mm day^{-1}), and relative mean bias error (rMBE, %). These parameters were calculated via the following equations:

$$R^2 = \frac{\left(\sum_{i=1}^n (ET_{p, \text{Penman}, i} - ET_{p, \text{Penman}})(ET_{p, \text{others}, i} - ET_{p, \text{others}}) \right)^2}{\left(\sum_{i=1}^n (ET_{p, \text{Penman}, i} - ET_{p, \text{Penman}})^2 \sum_{i=1}^n (ET_{p, \text{others}, i} - ET_{p, \text{others}})^2 \right)} \quad (10)$$

$$RMSE = \sqrt{\frac{1}{n} \sum_{i=1}^n (ET_{p, \text{Penman}, i} - ET_{p, \text{others}, i})^2} \quad (11)$$

$$rMBE = \left(\frac{1}{ET_{p, \text{Penman}}} \right) \times \frac{1}{n} \sum_{i=1}^n (ET_{p, \text{Penman}, i} - ET_{p, \text{others}, i}) \times 100 \quad (12)$$

where $ET_{p, \text{Penman}, i}$ and $ET_{p, \text{others}, i}$ are the i -th day ETp calculated by Penman model and other ETp models aforementioned, respectively. A high-performing model will have R^2 close to 1, RMSE close to 0 mm day^{-1} , and rMBE close to 0%.

2.7. Future ETp projection

Both the validated RF-based (RF1, RF2, and RF3) and the four empirical (JH, Mak, HS, and Ab) ETp models were used to project future ETp with downscaled daily climatic data from 34 GCMs under RCP4.5 and RCP8.5 climate scenarios. Daily ETp values were then summed to obtain annual ETp for each GCM at the eight stations. The ETp change for a certain future period was the difference between the mean annual ETp for that period and the mean annual ETp for the baseline period.

2.8. Contribution analysis of uncertainty in future ETp projections

The analysis of variance (ANOVA) technique has been widely used to quantify the contribution of different sources in uncertainty analysis (Aryal et al., 2019; Su et al., 2017; Tao et al., 2018; Wang et al., 2018a). This technique is able to partition the total observed variances into different sources, thus identifying the contribution of different sources to the total variance. Compared with other commonly used methods (e.g., recursive models, parameter identification, and Bayesian approaches) in uncertainty analysis (Ashraf Vaghefi et al., 2019; Freni et al., 2009), the ANOVA method requires fewer assumptions and considers the interactive contributions of different sources of the uncertainty to the total variance (Ashraf Vaghefi et al., 2019; Yip et al., 2011). Thus, we used a three-way (three factors) ANOVA to quantify the relative contribution of GCMs, RCPs, and ETp models to the uncertainty in ETp projections. A three-way ANOVA can be split into

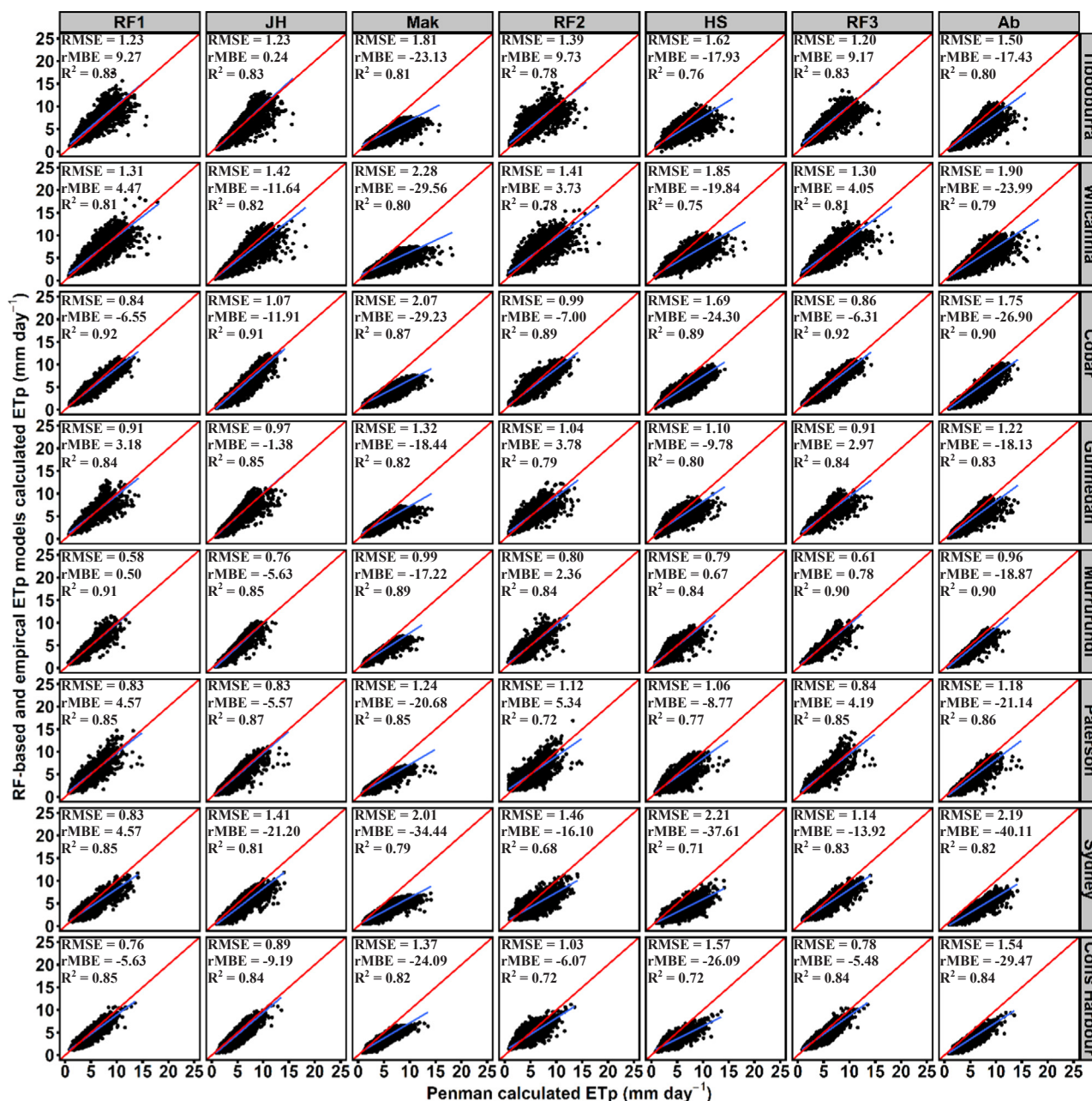


Fig. 2. Scatter plots of the Penman-calculated daily ETp (mm day⁻¹) vs ETp calculated by RF-based and empirical ETp models during the model testing stage (2001–2014) for each of eight stations in New South Wales, Australia. The units for RMSE and rMBE are mm day⁻¹ and %, respectively. Blue lines are linear regression lines and red lines are 1:1 lines.

seven fractions that include the three main effects and the four interaction effects. The total sum of squares (SST) was calculated as:

$$\begin{aligned}
 SST &= SS_{GCMs} + \underbrace{SS_{RCpS} + SS_{ETp,models}}_{\text{main effects}} \\
 &+ \underbrace{SS_{GCMs:RCpS} + SS_{GCMs:ETp,models} + SS_{RCpS:ETp,models} + SS_{GCMs:RCpS:ETp,models}}_{\text{interaction effects}}
 \end{aligned}
 \tag{13}$$

3. Results

3.1. Performance of ETp models during the historical period

Historical ETp estimation (2001–2014, Fig. 2) indicated that RF-

based ETp models generally outperformed the corresponding empirical ETp models (i.e., empirical ETp models which required the same inputs). Specifically, RF-based ETp models generally produced greater R², smaller RMSE, and smaller absolute rMBE than the corresponding empirical ETp models did at nearly all eight stations. For example, consider the results for the RF1, JH, and Mak models. Their R² values all ranged from 0.80 to 0.90. However, the RMSE of RF1 ranged from 0.58 mm day⁻¹ to 1.31 mm day⁻¹, generally lower than that of JH (from 0.76 mm day⁻¹ to 1.42 mm day⁻¹) and Mak (from 0.99 mm day⁻¹ to 2.28 mm day⁻¹). Moreover, ETp values calculated by RF-based models generally followed the Penman model, while other empirical models (e.g., MaK and HS) tended to underestimate ETp (compare blue regression lines with red 1:1 lines in Fig. 2). Even at stations where nearly all RF-based and empirical models underestimated ETp, such as at Cobar and Sydney, RF-based models still

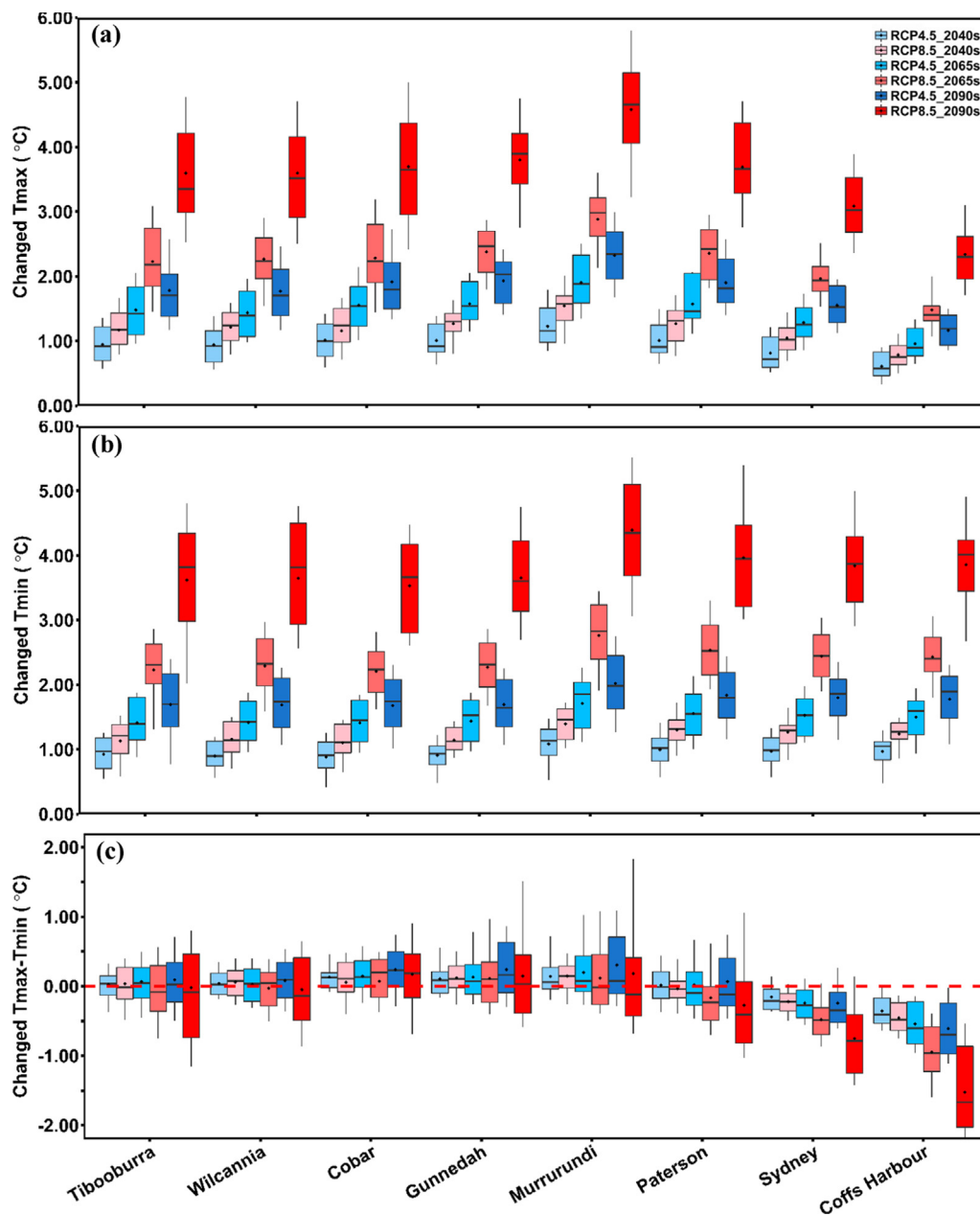


Fig. 3. Projected changes in T_{max} ($^{\circ}\text{C}$), T_{min} ($^{\circ}\text{C}$), $T_{max}-T_{min}$ ($^{\circ}\text{C}$), R_s ($\text{MJ m}^{-2} \text{ day}^{-1}$), and rainfall (mm year^{-1}) in the near future (2026–2050, 2040s), the medium future (2051–2075, 2065s), and the far future (2076–2100, 2090s) at eight stations in New South Wales, Australia, under RCP4.5 and RCP8.5 scenarios based on 34 GCMs compared with baseline values (1990–2014). Lower and upper box boundaries indicate the 25th and 75th percentiles, respectively. The black lines and dots inside the box mark the median and mean, respectively. The lower and upper whiskers indicate the 10th and 90th percentiles, respectively.

performed better, showing better consistency with the Penman model. The better performance of RF-based models may be explained by their ability to deal with non-linear processes between response variable and predictors. In addition, RF1 and RF3 showed similar performance at the eight stations, indicating that T_{min} might not be a key factor influencing the accuracy of RF-based ETp models. Again, these two models performed better than RF2 which might denote that R_s instead of R_a was a more important factor for estimating ETp with RF-based ETp models.

3.2. The change of climatic factors under future climate scenarios

Consistent increases were observed in T_{max} (Fig. 3a) and T_{min} (Fig. 3b) irrespective of RCP scenarios and stations. Specifically, the increases of mean T_{max} ranged from 0.61 $^{\circ}\text{C}$ by the 2040s to 2.33 $^{\circ}\text{C}$ by the 2090s under RCP4.5 while the range for mean T_{min} was 0.88 $^{\circ}\text{C}$

(2040s) to 2.02 $^{\circ}\text{C}$ (2090s). Under RCP8.5, larger increases were found in both T_{max} and T_{min} than under RCP4.5 for a certain future period. For instance, the range of increases of mean T_{max} and mean T_{min} under RCP8.5 were 0.79 $^{\circ}\text{C}$ (2040s) to 4.58 $^{\circ}\text{C}$ (2090s) and 1.10 $^{\circ}\text{C}$ (2040s) to 4.39 $^{\circ}\text{C}$ (2090s), respectively. Moreover, as time increased into the future period, the increase in T_{max} and T_{min} became larger. Similar increasing trends were also found in R_s , independent of stations. Mean R_s (Fig. 3d) was projected to increase by 0.08–0.32 $\text{MJ m}^{-2} \text{ day}^{-1}$ under RCP4.5 and 0.01–0.29 $\text{MJ m}^{-2} \text{ day}^{-1}$ under RCP8.5.

In contrast to the uniform increase in T_{max} and T_{min} was the obvious difference found among stations in the direction and magnitude of change of ΔT over time (Fig. 3c). For instance, mean ΔT at Murrurundi increased by 0.14–0.31 $^{\circ}\text{C}$ under RCP4.5 and by 0.12–0.18 $^{\circ}\text{C}$ under RCP8.5 whereas it decreased by 0.36–0.61 $^{\circ}\text{C}$ under RCP4.5 and by 0.45–1.52 $^{\circ}\text{C}$ under RCP8.5 at Coffs Harbour. ΔT is related to the degree

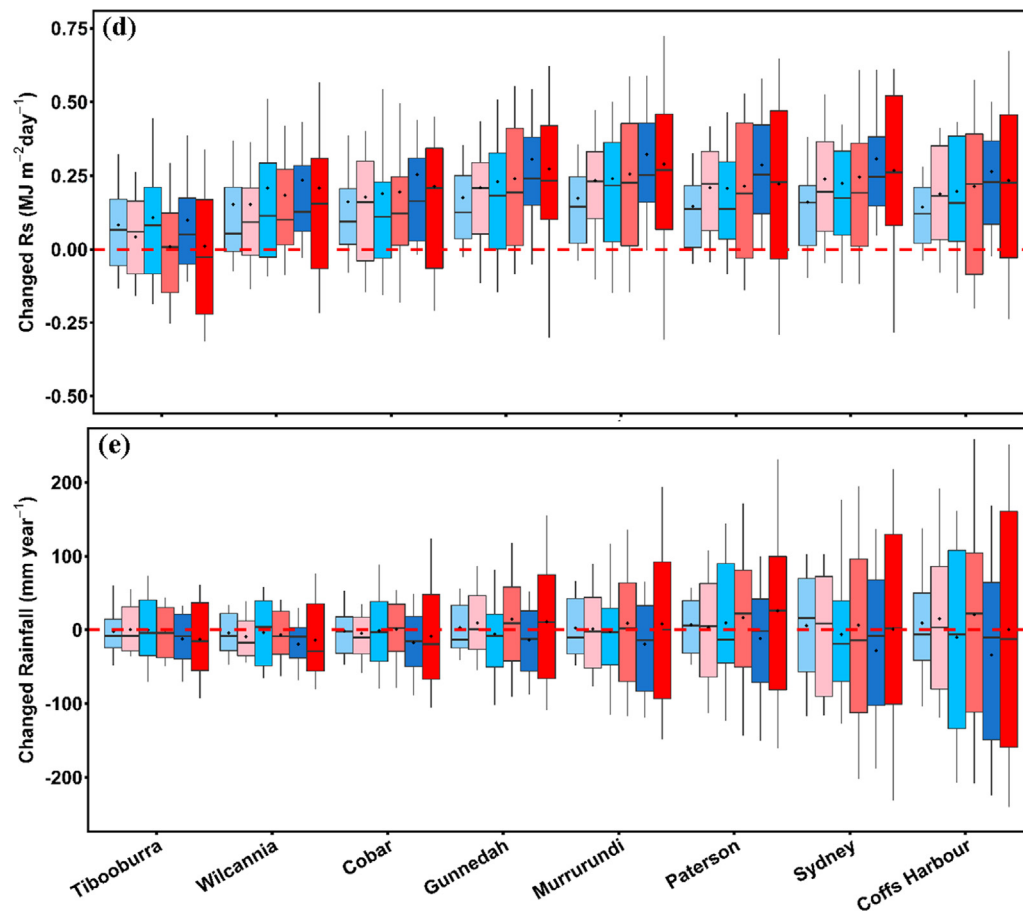


Fig. 3. (continued)

of cloud cover (Allen et al., 1998) and is a good indicator of solar radiation and relative humidity (Allen et al., 1998; Kingston et al., 2009). In particular, ΔT is an important input for the HS model. The variance change of ΔT may influence the change of ETp estimated by the HS model. There was no uniform direction in the change of rainfall over time (Fig. 3e). The ranges of mean rainfall change were -34 mm year^{-1} to 9 mm year^{-1} under RCP4.5 and from -14 mm year^{-1} to 26 mm year^{-1} under RCP8.5.

3.3. ETp and its change under future climate scenarios

As expected, ETp estimated by all models showed obvious increases under RCP4.5 and RCP8.5 scenarios at all stations except Coffs Harbour where the HS-calculated ETp showed a slight change (Fig. 4 & Fig. 5). However, both the future ETp (Fig. S3 & Fig. S4 provided in Supplementary material) and the increasing magnitude showed large differences among ETp models for each station regardless of RCP scenarios. In general, RF-based models projected higher future ETp and larger increases than empirical ETp models did for all stations. For instance, RF1 generally projected the largest increase of mean ETp among models for a given future period, ranging from 49 mm year^{-1} (3.2%, 2040s) to 164 mm year^{-1} (11.7%, 2090s) under the RCP4.5 scenario, and from 64 mm year^{-1} (4.1%, 2040s) to 346 mm year^{-1} (24.1%, 2090s) under the RCP8.5 scenario. In contrast, mean ETp projected by Mak generally showed the smallest increase, ranging from 27 mm year^{-1} (1.3%, 2040s) to 69 mm year^{-1} (4.9%, 2090s) under RCP4.5, and from 28 mm year^{-1} (1.4%, 2040s) to 113 mm year^{-1} (8.0%, 2090s) under RCP8.5. Influenced by the change differences of T_{\max} , T_{\min} , and R_s (Fig. 3a, 3b, and 3d, respectively), ETp projected by any given model also showed larger increases under the RCP8.5 scenario than under the RCP4.5 scenario for any given future period.

Again, ETp increases became larger as time into the future period increased. The ensemble increases of mean ETp across eight stations ranged from 33 mm year^{-1} (2.1%, 2040s) to 129 mm year^{-1} (9.2%, 2090s) under RCP4.5, and from 43 mm year^{-1} (2.8%, 2040s) to 248 mm year^{-1} (17.6%, 2090s) under RCP8.5.

3.4. Contribution of climatic factors to ETp change

In order to determine the relationships between the change of ETp and changes of meteorological factors, multiple linear regression was performed for each station using changes of T_{\max} , T_{\min} , R_s , and rainfall as independent variables and changes of ETp as the dependent variable. Our analysis showed that changes in T_{\max} , T_{\min} , R_s , and rainfall generally accounted for more than 92.0% of the ETp change, and the change of rainfall had only a slight influence in ETp for most stations (Table 4). We also found that relationships between the change of T_{\max} , T_{\min} , and R_s and the change of ETp could be grouped based on the input requirements of ETp models. In general, compared with T_{\max} and T_{\min} , a unit increase of R_s led to a larger increase of ETp projected by RF1, JH, and Mak. In contrast, the largest ETp increases (ranging from $64.0 \text{ mm year}^{-1}$ to $116.7 \text{ mm year}^{-1}$) projected by RF2 and HS were caused by a unit increase of T_{\max} , while changes in T_{\min} and R_s were negatively related to ETp changes. Lastly, for RF3 and Ab, one unit increase in R_s and T_{\max} could contribute roughly equally to the change in ETp.

3.5. Contribution of different sources to the uncertainty of ETp projections

Both ranges of future ETp and ETp differences among models and RCP scenarios indicated the existing uncertainty in future ETp projections. Thus, we used ANOVA to quantify the relative contributions of

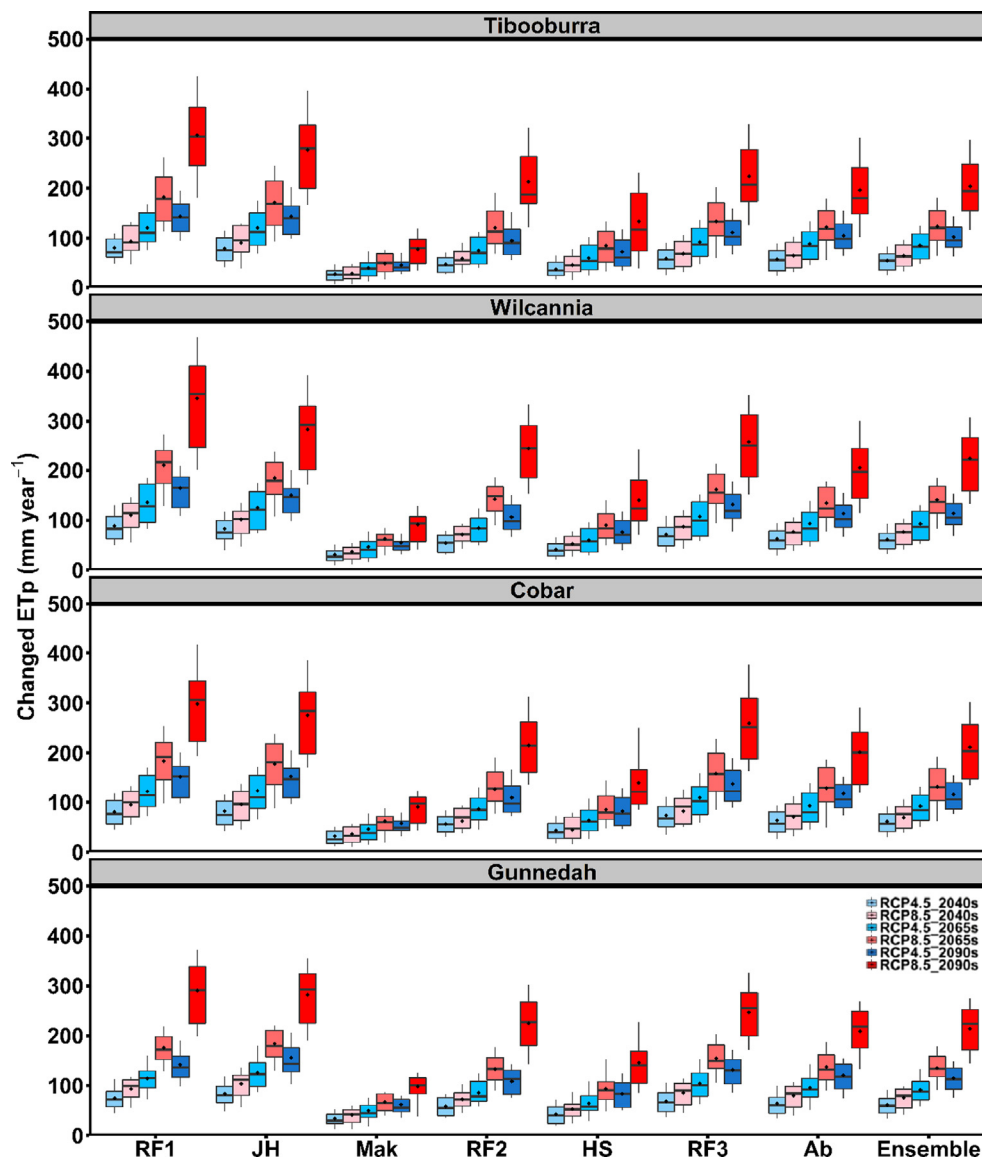


Fig. 4. Projected ETp changes for four arid/semi-arid stations in New South Wales, Australia in the near future (2026–2050, 2040s), the medium future (2051–2075, 2065s), and the far future (2076–2100, 2090s) under RCP4.5 and RCP8.5 scenarios based on 34 GCMs compared with baseline ETp (1990–2014). Lower and upper box boundaries indicate the 25th and 75th percentiles, respectively. The black lines and dots inside the box mark the median and mean, respectively. The lower and upper whiskers indicate the 10th and 90th percentiles, respectively.

GCMs, ETp models, and RCP scenarios to the uncertainty of ETp projections (Fig. 6). The RCPs accounted for around 40.0% of the uncertainty of ETp projections at all stations except the humid stations (Sydney, Coffs Harbour), indicating the dominant role of RCPs in the uncertainty of ETp projections. Following RCPs, the contribution of GCMs to uncertainty ranged from 16.7% to 28.8% among the eight stations. The ETp models contributed less than 16.0% to uncertainty at most stations. However, at Sydney and Coffs Harbour, the contribution of ETp models to uncertainty was roughly equal to or even higher than that observed for RCPs.

4. Discussion

Our study found that RF-based models produced ETp values that were much closer to Penman-calculated ETp during the historical period, indicating that RF-based ETp models generally outperformed empirical ETp models (Fig. 2 & Fig. S2). For the empirical ETp models, JH-calculated ETp was close to RF-calculated ETp during both the historical and future periods, whereas the rest of the empirical ETp

models produced relatively lower ETp (Fig. 2, Figs. S2–S4). Though the use of RF-based models for projecting future ETp is rare, their good performance in estimating historical evapotranspiration has been reported by other researchers (Fan et al., 2018; Feng et al., 2017). For instance, Feng et al. (2017) compared the performance of RF-based and generalized regression neural networks (GRNN)-based models in estimating daily ET_0 against the PM-FAO56 model based on two different input combinations. They found that the RF-based models (with R^2 ranging from 0.89 to 0.98) generally outperformed the GRNN-based models. Although there is no strong evidence to guarantee which model is more reliable for predicting future ETp (Kay and Davies, 2008), the use of RF-based ETp models is still advisable due to the following reasons. Firstly, these models have more flexibility for adding climatic inputs to improve their accuracy (Fan et al., 2018). Thus, when reliable climatic parameters are available, it is more feasible and efficient to train RF-based models than to calibrate empirical ETp models. Secondly, the testing and training of RF-based ETp models are more easily accomplished and it is possible to efficiently do cross-station validation. In contrast, one of the most commonly used methods to improve

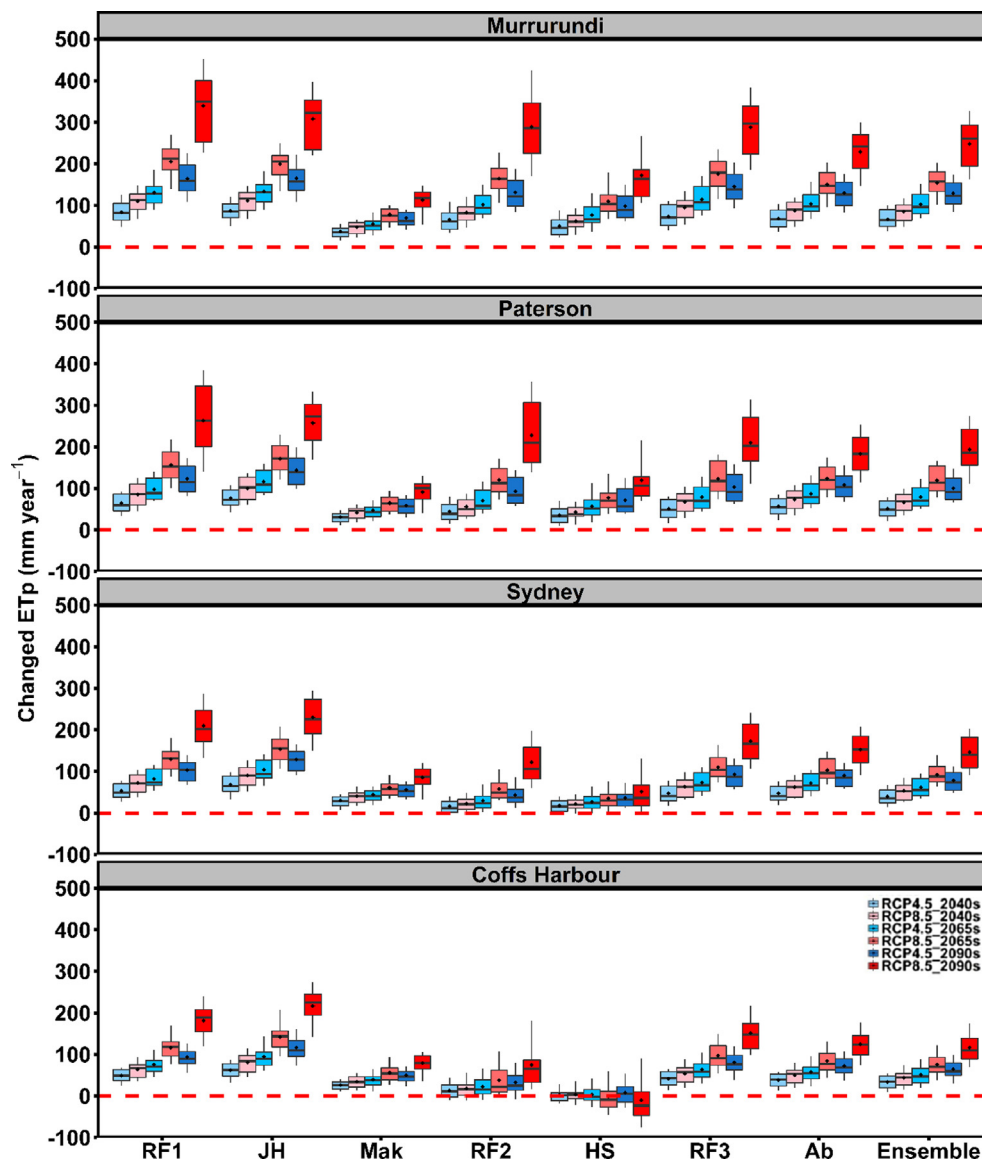


Fig. 5. Projected ETp changes for four humid/sub-humid stations in New South Wales, Australia, in the near future (2026–2050, 2040s), the medium future (2051–2075, 2065s), and the far future (2076–2100, 2090s) under RCP4.5 and RCP8.5 scenarios based on 34 GCMs compared with baseline ETp (1990–2014). The lower and upper box boundaries indicate the 25th and 75th percentiles, respectively. The black lines and dots inside the box mark the median and mean, respectively. The lower and upper whiskers indicate the 10th and 90th percentiles, respectively.

performance of simplified empirical models is to re-calibrate the empirical coefficients based on a linear relationship against observed ET or Penman-Monteith-type models (Droogers and Allen, 2002; Tabari and Talaei, 2011). However, these coefficients are generally location-specific and may result in less accurate performance in another region. Even if empirical coefficients are calibrated for a certain station, the updated coefficients may vary with time due to climatic changes and variations (Nouri and Homaei, 2018).

ETp projected by all models showed an overall increase under future climate scenarios and the increase was the largest at the end of the 21st century under the RCP8.5 scenario (Fig. 4 & Fig. 5). The increases in T_{\max} , T_{\min} , and R_s all contributed to the upward trend of ETp (Pan et al., 2015; Scheff and Frierson, 2014), as shown in Table 4. Although ETp increases under future climate scenarios have been widely reported (Dong et al., 2020; Gharbia et al., 2018; Pan et al., 2015; Scheff and Frierson, 2014; Tao et al., 2015; Wang et al., 2017b; Wang et al., 2015), large variances and uncertainties were observed in the magnitudes of the increases. At the global scale, Scheff and Frierson (2014) adopted the PM-FAO56 model with climatic data from 13 GCMs to project the

future ETp. They found ETp generally increased 10.0% to 45.0% by the end of the 21st century. Also at the global scale, Pan et al. (2015) adopted the Dynamic Land Ecosystem Model to project future global terrestrial evapotranspiration under the A2 and B1 emission scenarios. They found that compared with the 2000s, terrestrial evapotranspiration by the 2090s would increase 14.0% under the A2 scenario and 4.5% under the B1 scenario. In the Shannon River catchment, Ireland, Gharbia et al. (2018) adopted the Hamon model with climatic data from multi-GCMs to project future ETp and found that ETp could increase up to 13.5% by the 2080s compared with ETp in 1961–2014. In Australia, Johnson and Sharma (2010) used outputs from five GCMs to drive the PenPan model and projected open body water evaporation in the future. They claimed that the average increase in open body water evaporation in 2070 would be approximately 7% under the A2 scenario and 5% under the B1 scenario. In our study, the RF-based ETp models generally produced a roughly comparable increase in ETp to that of the above-mentioned studies, ranging from 2.1% to 11.7% under RCP4.5 and from 4.8% to 24.1% under RCP8.5 by the end of 21st century. As CSIRO and BOM (2015) indicated, there was high confidence in the

Table 4

Regression coefficients for changes in ETp (ΔETp , mm year⁻¹) with changes in maximum temperature (ΔT_{max} , °C), minimum temperature (ΔT_{min} , °C), solar radiation (ΔR_s , MJ m⁻² day⁻¹), and rainfall (ΔP , mm year⁻¹) in a multiple linear regression model ($\Delta ETp = a \Delta T_{max} + b \Delta T_{min} + c \Delta R_s + d \Delta P$); units for a and b are mm year⁻¹ °C⁻¹; units for c are mm year⁻¹ (MJ m⁻² d⁻¹)⁻¹; units for d are mm year⁻¹ mm⁻¹. ***:p < 0.001, **:p < 0.01; *:p < 0.05.

| Sites | Models | a | b | c | d | R ² | Sites | Models | a | b | c | d | R ² |
|------------|---------|---------|----------|-----------|-----------|----------------|---------------|----------|----------|----------|----------|----------|----------------|
| Tibooburra | RF1 | 37.3*** | 45.5*** | 69.9*** | -0.010 | 0.996 | Murrurundi | RF1 | 56.4*** | 12.4*** | 51.6*** | 0.022 | 0.994 |
| | JH | 39.8*** | 36.5*** | 110.2*** | -0.001 | 0.999 | | JH | 36.9*** | 26.3*** | 81.0*** | -0.006 | 0.999 |
| | Mak | 11.0*** | 10.6*** | 78.7*** | 0.004 | 0.999 | | Mak | 11.9*** | 8.9*** | 70.9*** | -0.002 | 1.000 |
| | RF2 | 69.2*** | -12.6*** | -12.6** | -0.082** | 0.987 | | RF2 | 81.5*** | -22.0*** | -10.9* | 0.034 | 0.985 |
| | HS | 92.4*** | -54.5*** | -6.5** | -0.025* | 0.994 | | HS | 78.9*** | -42.6*** | -0.5 | 0.023*** | 0.996 |
| | RF3 | 63.5*** | -3.0** | 67.9*** | -0.044** | 0.997 | | RF3 | 65.4*** | -7.8*** | 47.8*** | 0.022* | 0.996 |
| | Ab | 57.6*** | -3.4*** | 86.5*** | -0.003 | 0.999 | | Ab | 50.4*** | -4.9*** | 70.5*** | 0.007 | 0.999 |
| Ensemble | 53.0*** | 2.7*** | 56.3*** | -0.023* | 0.998 | Ensemble | 54.5*** | -4.2*** | 44.4*** | 0.014* | 0.997 | | |
| Wilcannia | RF1 | 44.2*** | 45.4*** | 61.4*** | -0.040 | 0.997 | Paterson | RF1 | 55.4*** | 7.1* | 63.5*** | 0.043** | 0.981 |
| | JH | 39.2*** | 33.9*** | 94.5*** | -0.023* | 0.999 | | JH | 37.1*** | 25.4*** | 90.6*** | 0.002 | 0.999 |
| | Mak | 11.0*** | 10.2*** | 74.1*** | -0.003 | 1.000 | | Mak | 11.5*** | 8.5*** | 73.0*** | 0.000 | 1.000 |
| | RF2 | 64.0*** | 1.1 | -6.7* | -0.062* | 0.992 | | RF2 | 87.5*** | -29.4*** | -12.0 | 0.035 | 0.958 |
| | HS | 87.7*** | -47.3*** | -3.3* | -0.036* | 0.993 | | HS | 90.3*** | -54.0*** | 0.4 | 0.006 | 0.996 |
| | RF3 | 67.6*** | -0.5 | 60.5*** | -0.032** | 0.999 | | RF3 | 66.5*** | -15.9*** | 56.7*** | 0.022 | 0.984 |
| | Ab | 55.8*** | -3.0*** | 79.2*** | -0.017 | 0.999 | | Ab | 50.1*** | -4.3*** | 73.5*** | 0.003 | 0.999 |
| Ensemble | 52.8*** | 5.7*** | 51.4*** | -0.031** | 0.999 | Ensemble | 56.9*** | -8.9*** | 49.4*** | 0.016* | 0.993 | | |
| Cobar | RF1 | 48.4*** | 29.9*** | 49.6*** | -0.010 | 0.998 | Sydney | RF1 | 44.5*** | 12.2*** | 63.5*** | 0.017** | 0.992 |
| | JH | 37.0*** | 34.0*** | 94.5*** | -0.019* | 0.999 | | JH | 37.4*** | 23.9*** | 89.9*** | 0.003 | 0.999 |
| | Mak | 10.3*** | 10.6*** | 74.5*** | -0.003 | 1.000 | | Mak | 11.4*** | 8.3*** | 72.8*** | 0.000 | 1.000 |
| | RF2 | 72.5*** | -15.7*** | -4.6*** | -0.040*** | 0.997 | | RF2 | 85.2*** | -40.6*** | -11.3* | 0.018 | 0.919 |
| | HS | 87.3*** | -51.1*** | -4.3* | -0.029** | 0.991 | | HS | 101.2*** | -67.5*** | 0.3 | 0.012*** | 0.981 |
| | RF3 | 69.8*** | -3.5*** | 47.3*** | -0.025** | 0.999 | | RF3 | 62.4*** | -10.7*** | 61.7*** | 0.009* | 0.996 |
| | Ab | 53.1*** | -2.9** | 76.7*** | -0.016* | 0.998 | | Ab | 50.1*** | -5.1*** | 67.7*** | 0.004** | 0.999 |
| Ensemble | 54.0*** | 0.2 | 47.7*** | -0.020*** | 0.999 | Ensemble | 56.0*** | -11.3*** | 49.2*** | 0.009** | 0.996 | | |
| Gunnedah | RF1 | 34.6*** | 37.1*** | 56.7*** | -0.013 | 0.996 | Coffs Harbour | RF1 | 47.5*** | 13.3*** | 66.6*** | 0.007** | 0.998 |
| | JH | 39.5*** | 29.6*** | 91.5*** | -0.011 | 0.999 | | JH | 38.4*** | 27.1*** | 90.6*** | 0.001 | 0.999 |
| | Mak | 11.7*** | 9.5*** | 73.6*** | -0.002 | 1.000 | | Mak | 11.7*** | 9.2*** | 73.0*** | 0.000 | 1.000 |
| | RF2 | 70.2*** | -12.6*** | -5.3** | 0.006 | 0.992 | | RF2 | 116.7*** | -52.5*** | -15.8*** | 0.010 | 0.951 |
| | HS | 86.1*** | -49.3*** | -1.6 | 0.016* | 0.994 | | HS | 106.3*** | -66.0*** | -2.8 | 0.008** | 0.964 |
| | RF3 | 66.4*** | -6.6*** | 53.3*** | -0.003 | 0.998 | | RF3 | 68.7*** | -7.1*** | 60.7*** | 0.005* | 0.998 |
| | Ab | 53.8*** | -4.2*** | 74.5*** | 0.001 | 0.999 | | Ab | 51.9*** | -3.1*** | 67.8*** | 0.002* | 0.999 |
| Ensemble | 51.8*** | 0.5 | 49.0*** | -0.001 | 0.998 | Ensemble | 63.0*** | -11.3*** | 48.6*** | 0.005** | 0.998 | | |

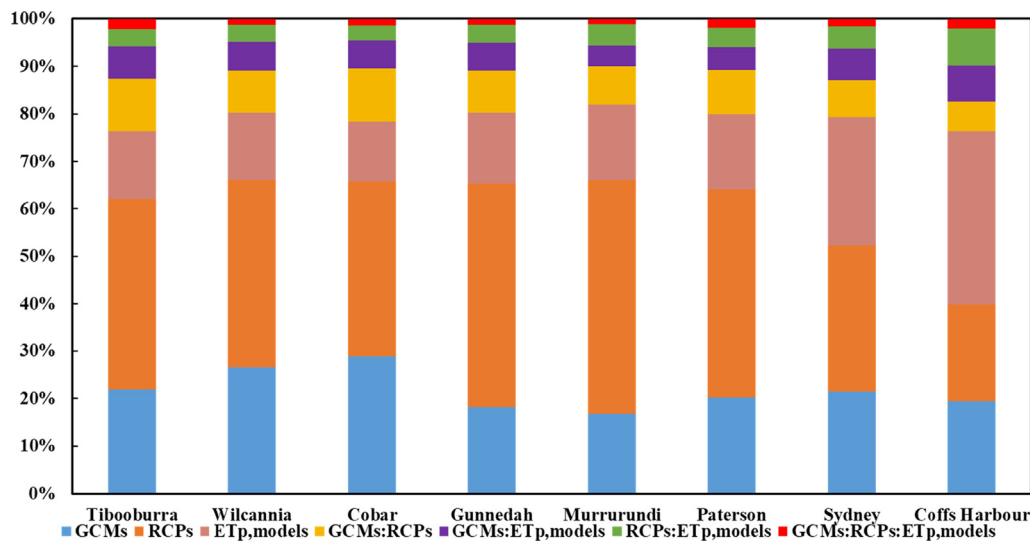


Fig. 6. The contribution of uncertainty sources to the change of ETp.

increase of ETp during this time period, but only medium confidence was found for the magnitude of the increase.

The large uncertainty in future ETp projections may be due to differences in GCMs (Teng et al., 2012), ETp models (Kingston et al., 2009), and RCPs (Wilby and Harris, 2006). Our study found that the dominant reason leading to uncertainty in ETp projection was attributable to the differences in the RCP scenarios, accounting for around 40% of the uncertainty (Fig. 6). This result is likely due to the fact that predicted changes of the major inputs (e.g., T_{max} , T_{min} , and R_s) for ETp models were clearly different under the different RCPs (Fig. 3). It is well

known that the GCMs we used in this study project raw monthly climatic data such as air temperature and solar radiation that include uncertainties and biases that are attributable to differences between GCMs and climate variables. However, we applied an improved statistical downscaling method (Liu and Zuo, 2012) that effectively corrected biases in the GCM-projected climate variables and matched observed climate while preserving the inter-annual and intra-seasonal variabilities of GCM projections (Liu et al., 2017). This approach effectively minimised the additional uncertainty from the downscaling method while the projected climate change signals were maintained for our

analysis of GCM uncertainties. In addition, we also found that the predictions of both climatic factors (Fig. 3) and ETp (Fig. 5-Fig. 6 & Figure S3-Figure S4) showed wider ranges under RCP8.5 than under RCP4.5, especially for the 2090s. This might indicate that GCMs behaved more differently from each other under RCP8.5 in the future (Shen et al., 2018), which might also contribute to the dominant role of RCPs in uncertainty of ETp projection. Following RCPs, GCM-related and ETp model-related uncertainty contributed roughly equally to ETp uncertainty, ranging from 10% to 30% (Fig. 6). Similar to our results, Kingston et al. (2009) projected global ETp with six alternative ETp models driven by data from five GCMs. They found that ETp model-related uncertainty was of a similar magnitude or, in some cases, greater than GCM-related uncertainty. Since ETp is an important input to hydrological models, the uncertainty in ETp projection may also influence hydrological projections (Thompson et al., 2014), thus reducing the confidence in predictions of water availability in the future. To deal with the uncertainty in future ETp projections, we recommend using multiple GCMs to drive various ETp models under different RCP scenarios, so that a relatively reliable projection is produced.

Quantifying the future increase in ETp can provide insights into future water availability and agricultural production in NSW. For instance, increased ETp indicates that atmospheric evaporative demand will be higher under future climate scenarios. However, both our study (Fig. 3e) and other studies (Chiew et al., 2009; Vaze and Teng, 2011) suggested that annual rainfall in NSW will not show significant increases in the future. With the combined influence of increasing ETp and normal or even decreased rainfall, there is a high possibility that runoff in NSW would decrease and this region would be drier (Teng et al., 2012). As Nicholls (2004) put it, rising temperatures and increasing ETp, even without decreasing rainfall, would increase the severity of droughts in Australia. Similarly, Feng et al. (2019a) projected changes of drought across the wheat belt of NSW with climatic data from 28 GCMs under RCP8.5. They found that decreasing rainfall combined with increasing temperature may lead to an expansion (from west to east) of the winter-spring drought-prone areas. Furthermore, we found that the increase in ETp at the traditionally arid stations (e.g. Tibooburra and Wilcannia, Fig. 4) was larger than at the humid stations (e.g., Sydney & Coffs Harbour, Fig. 5), which might indicate that the traditionally dry areas might become drier at a faster rate than the humid areas.

One limitation of this study is that we did not consider the influence of increasing atmospheric CO₂ on stomatal conductance. A higher CO₂ concentration will result in greater surface resistance (r_s). This may offset the magnitude of the ETp increases caused by the warming climate. In a recent study, Yang et al. (2019) developed an equation to describe the relationship between r_s and atmospheric CO₂ concentration. Based on the equation, they revised the PM-FAO56 model to consider the influence of increasing atmospheric CO₂. Their research offered a new perspective to assess the comprehensive impact of climate change on ETp and should be considered in future studies.

5. Conclusions

This study developed RF-based ETp models and assessed their performance against four empirical ETp models (JH, Mak, HS, and Ab), with the Penman-calculated ETp as a benchmark. The RF-based models and the four empirical ETp models were used to project ETp at eight stations across NSW using climatic data from 34 GCMs under the RCP4.5 and RCP8.5 scenarios. Study results indicated that RF-based models generally outperformed the empirical ETp models in estimating historical daily Penman ETp. All of these models projected that ETp would increase over time. However, the increased ETp estimates produced by the RF-based models better matched results obtained in other studies. The ensemble increases of mean ETp across eight stations ranged from 33 mm year⁻¹ (2.1%, 2040s) to 129 mm year⁻¹ (9.2%, 2090s) under RCP4.5, and from 43 mm year⁻¹ (2.8%, 2040s) to

248 mm year⁻¹ (17.6%, 2090s) under RCP8.5. Results of this study suggested that RF-based ETp models should be used for future ETp projections. Results also indicated that there is a higher possibility of water scarcity in NSW in the future, and adaptation measures will be necessary to deal with the effects of potential drought on agricultural production. Furthermore, differences in RCPs accounted for around 40% of the uncertainty in future ETp projections due to the great disparity in the expected temperature increases among the different emission scenarios. The large uncertainty in the projected increases of ETp highlights the necessity of adopting multiple model ensemble to project future ETp under different RCPs so that more reliable projections can be produced. For future work, other machine learning methods should be tested to project future ETp. Future studies should also consider the influence of increasing atmospheric CO₂ on ETp projections, and additional downscaling methods could be used to quantify their contribution to the uncertainty in ETp projections.

Declaration of Competing Interest

The authors declare that they have no known competing financial interests or personal relationships that could have appeared to influence the work reported in this paper.

Acknowledgements

The first author acknowledges the China Scholarship Council and University of Technology Sydney for a scholarship and the Wagga Wagga Agricultural Institute for providing office facilities to carry out this work. Meanwhile, this research was jointly supported by the International Partnership Program of the Chinese Academy of Sciences (161461KYSB20170013), Chinese Academy of Sciences "Light of West China" Program.

We thank the Scientific Information for Land Owners and the Bureau of Meteorology for offering the climatic data used in this work. We also thank the Program for Climate Model Diagnosis and Intercomparison (PCMDI) and the WCRP's Working Group on Coupled Modelling (WGCM) for their contribution in the achievement of the WCRP CMIP5 GCMs dataset. Support of this dataset was provided by the Office of Science, US department of Energy.

Appendix A. Supplementary data

Supplementary data to this article can be found online at <https://doi.org/10.1016/j.jhydrol.2020.124756>.

References

- Allen, R.G., Pereira, L.S., Raes, D., Smith, M., 1998. Crop evapotranspiration - Guidelines for computing Crop Water Requirements. FAO Irrigation & Drainage Paper 56, Rome, Italy.
- Almorox, J., Quej, V.H., Martí, P., 2015. Global performance ranking of temperature-based approaches for evapotranspiration estimation considering Köppen climate classes. *J. Hydrol.* 528, 514–522. <https://doi.org/10.1016/j.jhydrol.2015.06.057>.
- Arnell, N.W., Gosling, S.N., 2013. The impacts of climate change on river flow regimes at the global scale. *J. Hydrol.* 486, 351–364. <https://doi.org/10.1016/j.jhydrol.2013.02.010>.
- Aryal, A., Shrestha, S., Babel, M.S., 2019. Quantifying the sources of uncertainty in an ensemble of hydrological climate-impact projections. *Theor. Appl. Climatol.* 135 (1), 193–209. <https://doi.org/10.1007/s00704-017-2359-3>.
- Ashraf Vaghefi, S., et al., 2019. Regionalization and parameterization of a hydrologic model significantly affect the cascade of uncertainty in climate-impact projections. *Clim. Dyn.* 53 (5), 2861–2886. <https://doi.org/10.1007/s00382-019-04664-w>.
- Azhar, A.H., Perera, B.J.C., 2011. Evaluation of Reference Evapotranspiration Estimation Methods under Southeast Australian Conditions. *J. Irrig. Drain. Eng.* 137 (5), 268–279. [https://doi.org/10.1061/\(ASCE\)IR.1943-4774.0000297](https://doi.org/10.1061/(ASCE)IR.1943-4774.0000297).
- Bae, D.-H., Jung, I.-W., Lettenmaier, D.P., 2011. Hydrologic uncertainties in climate change from IPCC AR4 GCM simulations of the Chungju Basin, Korea. *Journal of Hydrology* 401 (1), 90–105. <https://doi.org/10.1016/j.jhydrol.2011.02.012>.
- Breiman, L., 2001. Random Forests. *Machine Learning*, 45(1): 5-32. DOI:10.1023/A:1010933404324.
- Chen, Z., Lei, H., Yang, H., Yang, D., Cao, Y., 2017. Historical and future trends in wetting

- and drying in 291 catchments across China. *Hydrol. Earth Syst. Sci.* 21 (4), 2233.
- Chiew, F.H.S., et al., 2009. Estimating climate change impact on runoff across southeast Australia: Method, results, and implications of the modeling method. *Water Resour. Res.* 45 (10). <https://doi.org/10.1029/2008WR007338>.
- CSIRO, BOM, 2015. Climate change in Australia information for Australia's natural resource management regions: technical report, CSIRO and Bureau of Meteorology, Australia.
- Dong, Q., et al., 2020. The response of reference evapotranspiration to climate change in Xinjiang, China: Historical changes, driving forces and future projections. *Int. J. Climatol.* (ja). <https://doi.org/10.1002/joc.5861>.
- Donohue, R.J., McVicar, T.R., Roderick, M.L., 2010. Assessing the ability of potential evaporation formulations to capture the dynamics in evaporative demand within a changing climate. *J. Hydrol.* 386 (1–4), 186–197. <https://doi.org/10.1016/j.jhydrol.2010.03.020>.
- Droogers, P., Allen, R.G., 2002. Estimating reference evapotranspiration under inaccurate data conditions. *Irrig. Drainage Systems* 16 (1), 33–45.
- Durack, P.J., Wijffels, S.E., Matear, R.J., 2012. Ocean salinities reveal strong global water cycle intensification during 1950 to 2000. *science*, 336(6080): 455–458.
- Fan, J., et al., 2018. Evaluation of SVM, ELM and four tree-based ensemble models for predicting daily reference evapotranspiration using limited meteorological data in different climates of China. *Agric. For. Meteorol.* 263, 225–241. <https://doi.org/10.1016/j.agrformet.2018.08.019>.
- Feng, P., et al., 2019a. Projected changes in drought across the wheat belt of southeastern Australia using a downscaled climate ensemble. *Int. J. Climatol.* 39 (2), 1041–1053. <https://doi.org/10.1002/joc.5861>.
- Feng, P., Wang, B., Liu, D.L., Yu, Q., 2019b. Machine learning-based integration of remotely-sensed drought factors can improve the estimation of agricultural drought in South-Eastern Australia. *Agric. Syst.* 173, 303–316. <https://doi.org/10.1016/j.agry.2019.03.015>.
- Feng, Y., Cui, N., Gong, D., Zhang, Q., Zhao, L., 2017. Evaluation of random forests and generalized regression neural networks for daily reference evapotranspiration modelling. *Agric. Water Manag.* 193, 163–173. <https://doi.org/10.1016/j.agwat.2017.08.003>.
- Feng, Y., Jia, Y., Zhang, Q., Gong, D., Cui, N., 2018. National-scale assessment of pan evaporation models across different climatic zones of China. *J. Hydrol.* 564, 314–328. <https://doi.org/10.1016/j.jhydrol.2018.07.013>.
- Freni, G., Mannina, G., Viviani, G., 2009. Urban runoff modelling uncertainty: Comparison among Bayesian and pseudo-Bayesian methods. *Environ. Modell. Software* 24 (9), 1100–1111. <https://doi.org/10.1016/j.envsoft.2009.03.003>.
- Gharbia, S.S., Smullen, T., Gill, L., Johnston, P., Pilla, F., 2018. Spatially distributed potential evapotranspiration modeling and climate projections. *Sci. Total Environ.* 633, 571–592. <https://doi.org/10.1016/j.scitotenv.2018.03.208>.
- Guio Blanco, C.M., Brito Gomez, V.M., Crespo, P., Liefß, M., 2018. Spatial prediction of soil water retention in a Páramo landscape: Methodological insight into machine learning using random forest. *Geoderma* 316, 100–114. <https://doi.org/10.1016/j.geoderma.2017.12.002>.
- Guo, D., Westra, S., Maier, H.R., 2017. Sensitivity of potential evapotranspiration to changes in climate variables for different Australian climatic zones. *Hydrol. Earth Syst. Sci.* 21 (4), 2107–2126. <https://doi.org/10.5194/hess-21-2107-2017>.
- Hargreaves, G.L., Hargreaves, G.H., Riley, J.P., 1985. Irrigation Water Requirements for Senegal River Basin. *J. Irrig. Drain. Eng.* 111 (3), 265–275. [https://doi.org/10.1061/\(ASCE\)0733-9437\(1985\)111:3\(265\)](https://doi.org/10.1061/(ASCE)0733-9437(1985)111:3(265)).
- Heung, B., Bulmer, C.E., Schmidt, M.G., 2014. Predictive soil parent material mapping at a regional-scale: A Random Forest approach. *Geoderma* 214–215, 141–154. <https://doi.org/10.1016/j.geoderma.2013.09.016>.
- Howden, M., Schroeter, S., Crimp, S., Hanigan, I., 2014. The changing roles of science in managing Australian droughts: An agricultural perspective. *Weather Clim. Extremes* 3, 80–89. <https://doi.org/10.1016/j.wace.2014.04.006>.
- Irmak, S., Kabenge, I., Skaggs, K.E., Mutiibwa, D., 2012. Trend and magnitude of changes in climate variables and reference evapotranspiration over 116-yr period in the Platte River Basin, central Nebraska-USA. *J. Hydrol.* 420–421, 228–244. <https://doi.org/10.1016/j.jhydrol.2011.12.006>.
- Jensen, M.E., Haise, H.R., 1963. Estimating evapotranspiration from solar radiation. *Proceedings of the American Society of Civil Engineers, Journal of the Irrigation and Drainage Division*, 89: 15–41.
- Johnson, F., Sharma, A., 2010. A comparison of Australian open water body evaporation trends for current and future climates estimated from class a evaporation pans and general circulation models. *J. Hydrometeorol.* 11 (1), 105–121. <https://doi.org/10.1175/2009jhm1158.1>.
- Kay, A., Davies, H., 2008. Calculating potential evaporation from climate model data: A source of uncertainty for hydrological climate change impacts. *J. Hydrol.* 358 (3–4), 221–239.
- Kingston, D.G., Todd, M.C., Taylor, R.G., Thompson, J.R., Arnell, N.W., 2009. Uncertainty in the estimation of potential evapotranspiration under climate change. *Geophys. Res. Lett.* 36 (20). <https://doi.org/10.1029/2009GL042627>.
- Kisi, O., 2015. Pan evaporation modeling using least square support vector machine, multivariate adaptive regression splines and M5 model tree. *J. Hydrol.* 528, 312–320. <https://doi.org/10.1016/j.jhydrol.2015.06.052>.
- Kişçi, Ö., 2013. Evolutionary neural networks for monthly pan evaporation modeling. *J. Hydrol.* 498, 36–45. <https://doi.org/10.1016/j.jhydrol.2013.06.011>.
- Kisi, O., Alizamir, M., 2018. Modelling reference evapotranspiration using a new wavelet conjunction heuristic method: Wavelet extreme learning machine vs wavelet neural networks. *Agric. For. Meteorol.* 263, 41–48. <https://doi.org/10.1016/j.agrformet.2018.08.007>.
- Liaw, A., Wiener, M., 2002. Classification and regression by randomForest. *R news* 2 (3), 18–22.
- Liu, D.L., et al., 2017. Effects of different climate downscaling methods on the assessment of climate change impacts on wheat cropping systems. *144(4): 687-701*. DOI:10.1007/s10584-017-2054-5.
- Liu, D.L., Zuo, H., 2012. Statistical downscaling of daily climate variables for climate change impact assessment over New South Wales, Australia. *Climatic Change* 115 (3–4), 629–666. <https://doi.org/10.1007/s10584-012-0464-y>.
- Lu, X., et al., 2018. Daily pan evaporation modeling from local and cross-station data using three tree-based machine learning models. *J. Hydrol.* 566, 668–684. <https://doi.org/10.1016/j.jhydrol.2018.09.055>.
- Mahringer, W., 1970. Verdunstungsstudien am neusiedler See. *Archiv für Meteorologie, Geophysik und Bioklimatologie, Serie B* 18 (1), 1–20.
- Makkink, G., 1957. Testing the Penman formula by means of lysimeters. *J. Inst. Water Eng.* 11, 277–288.
- McMahon, T., Finlayson, B., Peel, M., 2016. Historical developments of models for estimating evaporation using standard meteorological data. *Wiley Interdiscip. Rev.: Water* 3 (6), 788–818.
- Mehdizadeh, S., 2018. Estimation of daily reference evapotranspiration (ET₀) using artificial intelligence methods: Offering a new approach for lagged ET₀ data-based modeling. *J. Hydrol.* 559, 794–812. <https://doi.org/10.1016/j.jhydrol.2018.02.060>.
- Milly, P.C.D., Dunne, K.A., 2016. Potential evapotranspiration and continental drying. *Nat. Clim. Change* 6, 946. <https://doi.org/10.1038/nclimate3046>. <https://www.nature.com/articles/nclimate3046#supplementary-information>.
- Nicholls, N., 2004. The changing nature of Australian droughts. *Clim. Change* 63 (3), 323–336. <https://doi.org/10.1023/B:CLIM.0000018515.46344.6d>.
- Nouri, M., Homae, M., 2018. On modeling reference crop evapotranspiration under lack of reliable data over Iran. *J. Hydrol.* 566, 705–718. <https://doi.org/10.1016/j.jhydrol.2018.09.037>.
- Pan, S., et al., 2015. Responses of global terrestrial evapotranspiration to climate change and increasing atmospheric CO₂ in the 21st century. *Earth's Future* 3 (1), 15–35. <https://doi.org/10.1002/2014EF000263>.
- Penman, H.L., 1948. Natural evaporation from open water, bare soil and grass. *Proc. R. Soc. Lond. A* 193 (1032), 120–145.
- Priestley, C.H.B., Taylor, R.J., 1972. On the Assessment of Surface Heat Flux and Evaporation Using Large-Scale Parameters. *Mon. Weather Rev.* 100 (2), 81–92. [https://doi.org/10.1175/1520-0493\(1972\)100<0081:Otaosh>2.3.Co;2](https://doi.org/10.1175/1520-0493(1972)100<0081:Otaosh>2.3.Co;2).
- Randall, D.A., et al., 2007. Climate models and their evaluation, *Climate change 2007: The physical science basis. Contribution of Working. In: Group I to the Fourth Assessment Report of the IPCC (FAR)*. Cambridge University Press, pp. 589–662.
- Ravazzani, G., et al., 2014. Investigation of climate change impact on water resources for an alpine basin in Northern Italy: Implications for evapotranspiration modeling complexity. *PLoS One* 9 (10), e109053. <https://doi.org/10.1371/journal.pone.0109053>.
- Samani, Z., 2000. Estimating solar radiation and evapotranspiration using minimum climatological data. *J. Irrig. Drain. Eng.* 126 (4), 265–267. [https://doi.org/10.1061/\(ASCE\)0733-9437\(2000\)126:4\(265\)](https://doi.org/10.1061/(ASCE)0733-9437(2000)126:4(265)).
- Scheff, J., Frierson, D.M.W., 2014. Scaling potential evapotranspiration with greenhouse warming. *J. Clim.* 27 (4), 1539–1558. <https://doi.org/10.1175/jcli-d-13-00233.1>.
- Sheffield, J., Wood, E.F., Roderick, M.L., 2012. Little change in global drought over the past 60 years. *Nature* 491 (7424), 435.
- Shen, M., et al., 2018. Estimating uncertainty and its temporal variation related to global climate models in quantifying climate change impacts on hydrology. *J. Hydrol.* 556, 10–24. <https://doi.org/10.1016/j.jhydrol.2017.11.004>.
- Shiri, J., et al., 2012. Daily reference evapotranspiration modeling by using genetic programming approach in the Basque Country (Northern Spain). *J. Hydrol.* 414–415, 302–316. <https://doi.org/10.1016/j.jhydrol.2011.11.004>.
- Su, B., Huang, J., Zeng, X., Gao, C., Jiang, T., 2017. Impacts of climate change on streamflow in the upper Yangtze River basin. *Clim. Change* 141 (3), 533–546. <https://doi.org/10.1007/s10584-016-1852-5>.
- Tabari, H., Kisi, O., Ezani, A., Hosseinzadeh Talaei, P., 2012. SVM, ANFIS, regression and climate based models for reference evapotranspiration modeling using limited climatic data in a semi-arid highland environment. *J. Hydrol.* 444–445, 78–89. <https://doi.org/10.1016/j.jhydrol.2012.04.007>.
- Tabari, H., Talaei, P.H., 2011. Local calibration of the hargreaves and priestley-taylor equations for estimating reference evapotranspiration in arid and cold climates of Iran based on the penman-monteith model. *J. Hydrol. Eng.* 16 (10), 837–845. [https://doi.org/10.1061/\(ASCE\)HE.1943-5584.0000366](https://doi.org/10.1061/(ASCE)HE.1943-5584.0000366).
- Tao, F., et al., 2018. Contribution of crop model structure, parameters and climate projections to uncertainty in climate change impact assessments. *Glob. Change Biol.* 24, 1291–1307. <https://doi.org/10.1111/gcb.14019>.
- Tao, X.-E., Chen, H., Xu, C.-Y., Hou, Y.-K., Jie, M.-X., 2015. Analysis and prediction of reference evapotranspiration with climate change in Xiangjiang River Basin, China. *Water Sci. Eng.* 8 (4), 273–281. <https://doi.org/10.1016/j.wse.2015.11.002>.
- Teng, J., Vaze, J., Chiew, F.H.S., Wang, B., Perraud, J.-M., 2012. Estimating the relative uncertainties sourced from GCMs and hydrological models in modeling climate change impact on runoff. *J. Hydrometeorol.* 13 (1), 122–139. <https://doi.org/10.1175/jhm-d-11-058.1>.
- Thompson, J.R., Green, A.J., Kingston, D.G., 2014. Potential evapotranspiration-related uncertainty in climate change impacts on river flow: An assessment for the Mekong River basin. *J. Hydrol.* 510, 259–279. <https://doi.org/10.1016/j.jhydrol.2013.12.010>.
- Thompson, J.R., Green, A.J., Kingston, D.G., Gosling, S.N., 2013. Assessment of uncertainty in river flow projections for the Mekong River using multiple GCMs and hydrological models. *J. Hydrol.* 486, 1–30. <https://doi.org/10.1016/j.jhydrol.2013.01.029>.
- Vaze, J., Teng, J., 2011. Future climate and runoff projections across New South Wales, Australia: results and practical applications. *Hydrol. Process.* 25 (1), 18–35. <https://doi.org/10.1002/hyp.9888>.

- doi.org/10.1002/hyp.7812.
- Vaze, J., et al., 2008. Future climate and runoff projections (~2030) for New South Wales and Australian Capital Territory. NSW Department of Water and Energy, Sydney.
- Verdon-Kidd, D.C., Kiem, A.S., 2009. Nature and causes of protracted droughts in southeast Australia: Comparison between the Federation, WWII, and Big Dry droughts. *Geophys. Res. Lett.* 36 (22). <https://doi.org/10.1029/2009gl041067>.
- Vicente-Serrano, S.M., et al., 2014. Reference evapotranspiration variability and trends in Spain, 1961–2011. *Global Planet. Change* 121, 26–40. <https://doi.org/10.1016/j.gloplacha.2014.06.005>.
- Wang, B., Liu, D.L., Waters, C., Yu, Q., 2018a. Quantifying sources of uncertainty in projected wheat yield changes under climate change in eastern Australia. *Clim. Change* 151 (2), 259–273. <https://doi.org/10.1007/s10584-018-2306-z>.
- Wang, B., et al., 2018b. Estimating soil organic carbon stocks using different modelling techniques in the semi-arid rangelands of eastern Australia. *Ecol. Ind.* 88, 425–438. <https://doi.org/10.1016/j.ecolind.2018.01.049>.
- Wang, L., Kisi, O., Zounemat-Kermani, M., Li, H., 2017a. Pan evaporation modeling using six different heuristic computing methods in different climates of China. *J. Hydrol.* 544, 407–427. <https://doi.org/10.1016/j.jhydrol.2016.11.059>.
- Wang, W., Li, C., Xing, W., Fu, J., 2017b. Projecting the potential evapotranspiration by coupling different formulations and input data reliabilities: The possible uncertainty source for climate change impacts on hydrological regime. *J. Hydrol.* 555, 298–313. <https://doi.org/10.1016/j.jhydrol.2017.10.023>.
- Wang, W., Xing, W., Shao, Q., 2015. How large are uncertainties in future projection of reference evapotranspiration through different approaches? *J. Hydrol.* 524, 696–700. <https://doi.org/10.1016/j.jhydrol.2015.03.033>.
- Wilby, R.L., Harris, I., 2006. A framework for assessing uncertainties in climate change impacts: Low-flow scenarios for the River Thames, UK. *Water Resour. Res.* 42 (2). <https://doi.org/10.1029/2005wr004065>.
- Xu, Y.-P., Pan, S., Fu, G., Tian, Y., Zhang, X., 2014. Future potential evapotranspiration changes and contribution analysis in Zhejiang Province, East China. *J. Geophys. Res. Atmos.* 119 (5), 2174–2192. <https://doi.org/10.1002/2013jd021245>.
- Yang, Y., Roderick, M.L., Zhang, S., McVicar, T.R., Donohue, R.J., 2019. Hydrologic implications of vegetation response to elevated CO₂ in climate projections. *Nat. Clim. Change* 9 (1), 44–48. <https://doi.org/10.1038/s41558-018-0361-0>.
- Yip, S., Ferro, C.A.T., Stephenson, D.B., Hawkins, E., 2011. A Simple, Coherent Framework for Partitioning Uncertainty in Climate Predictions. DOI:10.1175/2011jcli4085.1.
- Zheng, H., et al., 2017. Assessing the ability of potential evapotranspiration models in capturing dynamics of evaporative demand across various biomes and climatic regimes with ChinaFLUX measurements. *J. Hydrol.* 551, 70–80. <https://doi.org/10.1016/j.jhydrol.2017.05.056>.